Application of Relativistic Mean Field Theory in Nuclear Physics

T. K. Jha*
Physics Department, Birla Institute of Technology and Science, Pilani
K. K. Birla Goa Campus, Zuarinagar - 403 726, Goa, INDIA

Over the last more than three decades, relativistic mean-field theories has grabbed attention for its applicability and effectiveness, that has led to our understanding of the fundamental physical world. Here we lineate the success of the theory by presenting results in both infinite nuclear matter as well as finite nuclei.

1. Introduction

Although QCD is believed to be the ultimate microscopic theory, but not much of a success has been achieved in explaining various aspects of strong nuclear interactions from the first principles of QCD. With the emergence of the concept of effective field theory (EFT) during **1990's**, introduced by Weinberg [1], emphasized EFT to be consistent with QCD and hence can represent the nuclear dynamics at this ground level. To understand the force between two or more nucleons remains the primary goal of nuclear physics. One also studies nuclear matter, a hypothetical nuclear systems with equal number of protons and neutrons uniformly distributed with no coulomb interaction. The only physical parameters to characterize such a system is the bulk binding energy and the saturation density, letting the total number of nucleons $A = N + Z$ go to infinity. The bulk binding energy is then $(E/\rho_0) - M = \Big(B/A\Big) \approx -16.0MeV$, which corresponds to Fermi momenta $(k_F) \approx 1.3\ fm^{-1}$. Nuclear Matter exists in different forms and structures depending on temperature and density. The well known renormalizable quantum field theory was introduced by Walecka [2] based on baryons and a scalar and vector meson, and its extensions have been phenomenal in explaining the various facets of nuclear matter. To study them, we revert to the mean field theory (MFT), where the meson field operators can be replaced by their vacuum expectation value or as the classical fields.

*Electronic address: tkjha@bits-goa.ac.in

2. Application to Infinite Nuclear Matter

The framework of Quantum Hadrodynamics [2, 3] laid down the pillars of relativistic theories which seem to provide solution to the so called "*the Coester band*" problem [4, 5]. Since our present knowledge of nuclear matter is confined around nuclear saturation density ($\rho_0 \approx 3 \times 10^{14} gcm^{-3}$) and therefore, in order to have some meaningful correlations while extrapolating to higher densities, the nuclear equation of state (EOS) must satisfy the nuclear saturation properties. For example, the uncertainty at ρ_0 especially of the nucleon effective mass and the nuclear incompressibility [6, 7] gets more pronounced at higher densities $(3 - 10\ \rho_0)$which are relevant to astrophysical context. The nuclear incompressibility derived from nuclear measurements and astrophysical observations exhibit a broad range of values $K = (180 - 800)$ MeV [8]. Apart from that we also need to sort out the uncertainty in the determination of mass of the scalar meson (σ-meson). The estimate from the Particle Data Group quotes the mass of this scalar meson in the range $(400 - 1200)$ MeV [9]. Therefore, the need of the hour is to constrain the nuclear matter EOS.

A. The Effective Chiral Model: Equation of State at $T = 0$

Phenomenologically, parallel to the well known $\sigma - \omega$ model, preferably known as

the Walecka model, chiral models [10] developed and were applied to nuclear matter studies. Chiral symmetry is a symmetry of strong interactions in the limit of vanishing quark masses and is desirable in any relativistic theory. This symmetry is spontaneously broken in the ground state resulting in the finite vacuum expectation value $\langle\sigma\rangle = \sigma_0 = f_\pi$. Equivalently, the potential for the $\sigma-$ field attains a minimum at f_π [11, 12]. The value of f_π reflects the strength of the symmetry breaking and experimentally it is found to be $f_\pi \approx 131$ MeV [9].

Presently, for study of nuclear matter, we choose a model which embodies chiral symmetry and has minimum number of free parameters that reproduce the saturation properties. The model is very similar to the Walecka model and embodies higher orders of the scalar field in addition to the dynamically generated mass of the vector meson. The effective Lagrangian of the model interacting through the exchange of the pseudo-scalar meson π, the scalar meson σ, the vector meson ω and the iso-vector $\rho-$meson is given by [13]:

$$\begin{aligned}\mathcal{L} &= \bar{\psi}_B \left[\left(i\gamma_\mu\partial^\mu - g_\omega\gamma_\mu\omega^\mu - \frac{1}{2}g_\rho\vec{\rho}_\mu\cdot\vec{\tau}\gamma^\mu\right) - g_\sigma \left(\sigma + i\gamma_5\vec{\tau}\cdot\vec{\pi}\right)\right] \psi_B \\ &+\frac{1}{2}\left(\partial_\mu\vec{\pi}\cdot\partial^\mu\vec{\pi} + \partial_\mu\sigma\partial^\mu\sigma\right) - \frac{\lambda}{4}\left(x^2 - x_0^2\right)^2 - \frac{\lambda b}{6m^2}\left(x^2 - x_0^2\right)^3 - \frac{\lambda c}{8m^4}\left(x^2 - x_0^2\right)^4 \\ &-\frac{1}{4}F_{\mu\nu}F_{\mu\nu} + \frac{1}{2}{g_\omega B}^2 x^2\omega_\mu\omega^\mu - \frac{1}{4}\vec{R}_{\mu\nu}\cdot\vec{R}^{\mu\nu} + \frac{1}{2}m_\rho^2\vec{\rho}_\mu\cdot\vec{\rho}^\mu \ . \end{aligned} \quad (1)$$

The above Lagrangian represents the interaction of the nucleon isospin doublet ψ_B with the aforesaid mesons. The higher order terms of the scalar field is expressed in terms of the invariant combination of the two i.e., $x^2 = \vec{\pi}^2 + \sigma^2$. In the model, g_σ, g_ω and g_ρ are the usual meson-nucleon coupling strength of the scalar, vector and the iso-vector fields respectively. The interaction of the scalar and the pseudoscalar mesons with the vector boson generates a dynamical mass for the vector bosons through spontaneous breaking of the chiral symmetry with scalar field attaining the vacuum expectation value x_0. Then the mass of the nucleon (m), the scalar (m_σ) and the vector meson mass (m_ω), are related to x_0 through

$$m = g_\sigma x_0, \quad m_\sigma = \sqrt{2\lambda}x_0, \quad m_\omega = g_\omega x_0 \ . \quad (2)$$

To obtain the equation of state, we revert to the mean-field procedure in which, one assumes the mesonic fields to be uniform i.e., without any quantum fluctuations. This approach has been extensively used to obtain EOS for high density matter [14], and gets increasingly valid when the source terms are large [3]. The total energy density 'ε' and pressure 'P' of symmetric nuclear matter for a given baryon density is:

$$\begin{aligned}\varepsilon &= \frac{\gamma}{2\pi^2}\int_o^{k_F} k^2dk\sqrt{k^2 + m^{\star 2}} + \frac{m^2(1-Y^2)^2}{8c_\sigma} \\ &- \frac{b}{12c_\omega c_\sigma}(1-Y^2)^3 + \frac{c}{16m^2c_\omega^2c_\sigma}(1-Y^2)^4 \\ &+ \frac{c_\omega\rho_B^2}{2Y^2} \end{aligned}$$

$$\begin{aligned}P &= \frac{\gamma}{6\pi^2}\int_o^{k_F} \frac{k^4dk}{\sqrt{k^2 + m^{\star 2}}} - \frac{m^2(1-Y^2)^2}{8c_\sigma} \\ &+ \frac{b}{12c_\omega c_\sigma}(1-Y^2)^3 - \frac{c}{16m^2c_\omega^2c_\sigma}(1-Y^2)^4 \\ &+ \frac{c_\omega\rho_B^2}{2Y^2} \end{aligned} \quad (3)$$

The meson field equations for ω and σ-meson are solved self-consistently at a fixed baryon density to obtain the respective field strengths and the corresponding energy density and pressure is calculated.

B. Evaluation of model parameters

Here our primary aim is to evaluate the set of parameters of the model that satisfies the nuclear matter properties defined at normal nuclear matter density (ρ_0) and at zero temperature. Similar procedure has been adopted in Ref. [15] to evaluate the parameters of the mean-field models, which satisfies the nuclear matter saturation properties. The individual contributions to the energy density for symmetric nuclear matter can be abbreviated as,

$$\varepsilon = \varepsilon_k + \varepsilon_\sigma + \varepsilon_\omega = \rho_0(m - a_1). \qquad (4)$$

From the the equilibrium condition $P(\rho_0, 0) = 0$, we have,

$$\begin{aligned} P &= -\varepsilon + \rho_B \frac{\partial \varepsilon}{\partial \rho_B} \\ &= \frac{1}{3}(\varepsilon_k - m^\star \rho_S) - \varepsilon_\sigma + \varepsilon_\omega = 0 \quad (5) \end{aligned}$$

Consequently, the respective energy contributions can be expressed in terms of these specified values at the saturation density. Using eqn. (4) and eqn. (5), they are given as,

$$\varepsilon_\sigma = \frac{1}{2}\left[\rho_0(m - a_1) - \frac{1}{3}(2\varepsilon_k + m^\star \rho_s)\right] \quad (6)$$

and

$$\varepsilon_\omega = \frac{1}{2}\left[\rho_0(m - a_1) - \frac{1}{3}(4\varepsilon_k - m^\star \rho_s)\right], \quad (7)$$

where ρ_s is the scalar density defined as,

$$\rho_s = \frac{1}{\pi^2} m^\star \left[k_F E_F - ln\Big(\frac{k_F + E_F}{m^\star}\Big) m^{\star 2}\right]. \quad (8)$$

In the above equations, $m^\star = Ym$ is the effective nucleon mass and $E_F = \sqrt{k_F^2 + m^{\star 2}}$ is the effective energy of the nucleon carrying momenta k_F.

Finally, for studying asymmetric matter, we need to incorporate the effect of iso-vector $\rho-$meson and the coupling for the $\rho-$ meson has to be obtained by fixing the asymmetry energy coefficient $J \approx 32 \pm 4\ MeV$ [16] at ρ_0. Accordingly, the $\rho-$ meson coupling constant (C_ρ) can be fixed using the relation,

$$J = \frac{c_\rho k_F^3}{12\pi^2} + \frac{k_F^2}{6\sqrt{(k_F^2 + m^{\star 2})}}, \qquad (9)$$

where $c_\rho \equiv g_\rho^2/m_\rho^2$ and $k_F = (6\pi^2 \rho_B/\gamma)^{1/3}$.

Thus the model parameters are evaluated self-consistently, for the specified or desired values of the properties of symmetric nuclear matter at saturation point. Further the nuclear incompressibility is then evaluated as,

$$K = 9\ \rho_0^2\ \frac{\partial^2(\varepsilon/\rho_B)}{\partial \rho_B}\Big|_0. \qquad (10)$$

C. Equation of state at $T \neq 0$

The study of finite temperature nuclear EOS is not only relevant to the medium energy heavy-ion collisions, but has also astrophysical implications. For example the phenomenon of liquid-gas phase transition at low temperature and density is perceived to happen in the crust of neutron star[17]. The liquid gas phase also has been studied by many authors based on the RMF theory[18]. The linear Walecka model estimates the critical temperature in the symmetric nuclear matter to be 18.3 MeV[3], which drops down to 14.2 MeV, if the non-linear terms were included in the model. However, recent experiments in heavy-ion collisions for dilute warm nuclear matter report a small liquid gas phase region and low critical temperature$\sim 13.1 \pm 0.6$ MeV[19].

The EOS for finite temperature can be defined in the same manner as zero temperature, and are given by:

$$\begin{aligned}\varepsilon(T) &= \frac{m^2(1-Y^2)^2}{8c_\sigma} - \frac{b}{12c_\omega c_\sigma}(1-Y^2)^3 \\ &+ \frac{c}{16m^2c_\omega^2c_\sigma}(1-Y^2)^4 + \frac{c_\omega n_B^2}{2Y^2} \\ &+ \frac{\gamma}{2\pi^2}\int_o^\infty k^2dk\sqrt{k^2+m^{\star 2}}(f(T)+\bar{f}(T))\end{aligned}$$

$$\begin{aligned}P(T) &= -\frac{m^2(1-Y^2)^2}{8c_\sigma} + \frac{b}{12c_\omega c_\sigma}(1-Y^2)^3 \\ &- \frac{c}{16m^2c_\omega^2c_\sigma}(1-Y^2)^4 + \frac{c_\omega n_B^2}{2Y^2} \\ &+ \frac{\gamma}{6\pi^2}\int_o^\infty \frac{k^4dk}{\sqrt{k^2+m^{\star 2}}}(f(T)+\bar{f}(T)) \quad (11)\end{aligned}$$

The vector and the scalar density at finite temperature are respectively modified as

$$\rho_B(T) = \frac{\gamma}{(2\pi)^3}\int_o^\infty d^3k(f(T)-\bar{f}(T)), \quad (12)$$

and

$$\rho_S(T) = \frac{\gamma}{(2\pi)^3}\int_o^\infty \frac{m^* d^3k}{\sqrt{k^2+m^{\star 2}}}(f(T)+\bar{f}(T)), \quad (13)$$

where $f(T)$ and $\bar{f}(T)$ are the usual nucleon and anti-nucleon distribution function.

D. Neutron Star: Dense matter composition and Neutron star properties

To have a realistic description of the dense neutron star matter, generalized the Lagrangian to include the lowest lying octet of baryons $(n, p, \Lambda^0, \Sigma^{-,0,+}, \Xi^{-,0})$ interacting through the exchange of the pseudo-scalar meson π, the scalar meson σ, the vector meson ω and the iso-vector $\rho-$meson and employed the the mean-field procedure to evaluate the meson fields in our present calculations. The total energy density 'ε' and pressure 'P' for a given baryon density in terms of the dimensionless variable $Y = x/x_0$ is given as:

$$\begin{aligned}\varepsilon &= \frac{2}{\pi^2}\int_0^{k_B} k^2dk\sqrt{k^2+m_B^{\star 2}} + \frac{m_B^2(1-Y^2)^2}{8c_{\sigma B}} \\ &- \frac{m_B^2 B}{12c_{\omega B}c_{\sigma B}}(1-Y^2)^3 + \frac{m_B^2 C}{16c_{\omega B}^2c_{\sigma B}}(1-Y^2)^4 \\ &+ \frac{1}{2Y^2}c_{\omega_B}\rho_B^2 + \frac{1}{2}m_\rho^2\rho_{03}^2 \\ &+ \frac{1}{\pi^2}\sum_{\lambda=e,\mu^-}\int_0^{k_\lambda} k^2dk\sqrt{k^2+m_\lambda^2}\,, \quad (14)\end{aligned}$$

$$\begin{aligned}P &= \frac{2}{3\pi^2}\int_0^{k_B}\frac{k^4dk}{\sqrt{k^2+m_B^{\star 2}}} - \frac{m_B^2(1-Y^2)^2}{8c_{\sigma B}} \\ &+ \frac{m_B^2 B}{12c_{\omega B}c_{\sigma B}}(1-Y^2)^3 - \frac{m_B^2 C}{16c_{\omega B}^2c_{\sigma B}}(1-Y^2)^4 \\ &+ \frac{1}{2Y^2}c_{\omega_B}\rho_B^2 + \frac{1}{2}m_\rho^2\rho_{03}^2 \\ &+ \frac{1}{3\pi^2}\sum_{\lambda=e,\mu^-}\int_0^{k_\lambda}\frac{k^4dk}{\sqrt{k^2+m_\lambda^2}} \quad (15)\end{aligned}$$

The terms with the subscript 'B' should be interpreted as sum over all the states of the baryonic octets. The meson field equations for the σ, ω and $\rho-$mesons are then solved self-consistently at a fixed baryon density to obtain the respective field strengths. The EOS for the $\beta-$equilibrated hyperon rich matter is obtained with the requirements of conservation of total baryon number and charge neutrality condition, which are given by

$$\sum_B Q_B\rho_B + \sum_l Q_l\rho_l = 0, \quad (16)$$

where ρ_B and ρ_l are the baryon and the lepton (e,μ) number densities with Q_B and Q_l as their respective electric charges.

We solve the above equations to study the structural properties of a static neutron star using the EOS derived for the electrically charge neutral hyperonic dense matter [20, 21].

In order to calculate the models of rotating star we employ the method based on the Komatsu-Eriguchi-Hachisu method to construct uniformly rotating star models [22].

3. Results and discussions

A. Evaluation of model parameters

Similar procedure has been employed to obtain the parameters of the model in the RMF theory too. Fig. 1, shows a few of the parameters with the respective saturation properties as obtained in the RMF model [23].

	NL3	NL3-II	NL1	NL-SH
M (MeV)	939	939	938	939
m_σ (MeV)	508.194	507.680	492.250	526.059
m_ω (MeV)	782.501	781.869	783.000	783.000
m_ρ (MeV)	763.000	763.000	763.000	763.000
g_σ	10.217	10.202	10.138	10.4444
g_ω	12.868	12.854	13.285	12.945
g_ρ	4.474	4.480	4.976	4.383
g_2 (fm^{-1})	−10.431	−10.391	−12.172	−6.9099
g_3	−28.885	−28.939	−36.265	−15.8337
Nuclear matter properties				
ρ_0 (fm^{-3})	0.148	0.149	0.153	0.146
$(E/A)_\infty$ (MeV)	16.299	16.280	16.488	16.346
K (MeV)	271.76	272.15	211.29	355.36
J (MeV)	37.4	37.7	43.7	36.1
m^*/m	0.60	0.59	0.57	0.60

FIG. 1: NL3, NL3-II, NL1 and NL-SH parameters of the relativistic mean-field model [23].

In the present calculation, we fix the saturation density to be $\rho_0 = 0.153 fm^{-3}$ [6], and the binding energy per nucleon is fixed at an empirical value $B/A - m = -16.3$ MeV. One can then exploit the uncertainty in the nucleon effective mass, and nuclear incompressibility to obtain a range of parameters. As followed from the model, the VEV of the scalar field which has a minimum potential at f_π is related to the vector coupling constant C_ω through the relation $x_0 = f_\pi = m_\omega/g_\omega = 1/\sqrt{C_\omega}$. The scalar meson mass is then given by $m_\sigma = m\ \sqrt{C}_\omega/\sqrt{C}_\sigma$. The obtained parameters, with the method described in the previous section, are enlisted in Table I. The calculated sigma meson mass is predicted within $(340 - 700)$ MeV corresponding to $m^\star/m = (0.75{-}0.90)$. Although, the values obtained from the analysis of neutron scattering off lead nuclei [6, 25] is consistent with the range $m^\star/m = (0.80 - 0.90)$, a lower nucleon effective mass is is known to reproduce the finite nuclei properties, such as the spin-orbit effects splitting correctly.

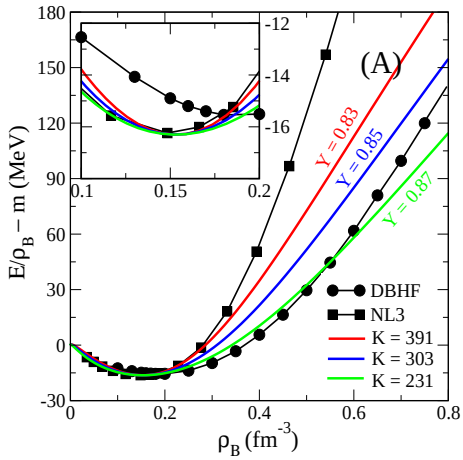

FIG. 2: Binding energy per nucleon of symmetric nuclear matter plotted as a function of baryon density up to nearly $5\rho_0$. For comparison, we also plot the same for NL3 parameter set from the Relativistic Mean Field theory [23] as well as EOS from DBHF [24] in the non-relativistic domain. The inset plot displays the curve in the vicinity of nuclear saturation.

B. Equation of state at $T = 0$

The resulting energy per nucleon for few selected parameters of sigma model for symmetric nuclear matter is calculated for these parameters and is plotted in Fig. 2. For comparison, we plot the same with NL3 parameterization from Relativistic Mean Field (RMF) calculations [23] and also the non-relativistic realistic DBHF (Bonn-A) parameterization [24]. In the inset, the region of saturation density is magnified, where we find nice agreement within relativistic mean-field models near ρ_0. The resulting EOS of effective sigma model seems to be soft at higher densities in comparison to that predicted by the NL3 parameter set which has $K = 271.7$ MeV.

C. EOS at $T \neq 0$

Here we analyze the effect of temperature on the EOS, explicitly near the nuclear mat-

TABLE I: Few parameters of the effective chiral model that satisfies the nuclear matter saturation properties. Other derived quantities such as the scalar meson mass 'm_σ', the pion decay constant 'f_π' and the nuclear matter incompressibility (K) at ρ_0 are also given.

set	c_σ (fm^2)	c_ω (fm^2)	c_ρ (fm^2)	B (fm^2)	C (fm^4)	m_σ (MeV)	Y	f_π (MeV)	K (MeV)
1	6.223	2.709	5.178	-0.711	0.748	619.585	0.80	119.890	560
2	**6.772**	**1.995**	**5.285**	**-4.274**	**0.292**	**509.644**	**0.85**	**139.710**	**303**
3	7.942	1.041	5.388	-6.908	15.197	339.910	0.90	193.437	163

ter density, to investigate Liquid-Gas phase transition. For this, one can make a smooth transition from liquid to gas state by making a Maxwell construction. At a particular temperature, the pocket vanishes and is marked as the pure gas state. At this point the pressure gradient with respect to density (inflection point) is zero ($\partial P/\partial n_B|_{T_c} = \partial^2 P/\partial {n_B}^2|_{T_c} = 0$) and is noted as the critical point for liquid gas phase transition.

The critical temperature obtained by the density dependent relativistic mean-field theory [26] (T_c =12.66 MeV) and the experimental value ($T_c = 13.1 \pm 0.6$ MeV) [19]. If one consider the original Walecka model [3] (no non-linear terms), the critical temperature is $T_c \approx 18.3$. This can be reduced to $T_c \approx 14.2$ MeV [27], when one introduces the non-linear terms in the scalar field.

The overall result of our calculations for the liquid-gas phase transition in case of symmetric nuclear matter is listed in Table II, where $T_c(MeV)$, $P_c(MeVfm^{-3})$ and $\rho_c(fm^{-3})$ are the critical temperature, critical pressure and critical density respectively, for the liquid-gas co-existence point [28]. The variation of the critical temperature with nuclear incompressibility of the nuclear matter can be seen from the table.

TABLE II: *Results for the liquid-gas phase transition in symmetric matter*

SET	M^*/M	$K(MeV)$	T_c	P_c	ρ_c
I	0.85	210	14.2	0.14	0.035
II	0.85	300	16.8	0.22	0.044
III	0.85	380	20.4	0.36	0.051

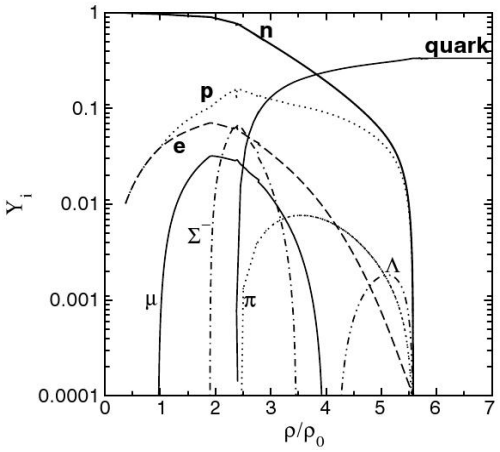

FIG. 3: Particle fractions of the baryons, leptons, and quarks obtained with E-RMF+CFL for $B^{1/4}$ = 188 MeV)[29].

D. Neutron Star Properties

Neutron stars are natural laboratories to study cold dense matter. Evidently, it opens up several important questions on the composition and structure of matter at $\approx (5-10)\rho_0$. A typical plot of particle fraction as a function of baryon density is shown in Fig. 3. Typically, the hyperons start appearing at around $2\rho_0$, where Σ^- appears first, closely followed by Λ^0. At higher densities other baryon thresholds are attained and they also start appearing. Such an analysis concludes

with the fact that the negatively charged particles are highly favored species in dense matter as evident from their respective order of appearance. Another interesting aspect is the deleptonization of matter at higher density. It can be seen that hyperons forms a sizable population in neutron star matter, and throws up interesting implication on the neutron star structure.

At high densities, quarks can also appear. In Fig. 3, the respective particle fraction of quarks as well as the octet of baryons is plotted, where quarks are in the color flavored locked phase [29], for a bag constant of 188 MeV. From the composition, one can find that the dense core of the stars may be rich in hyperons or quarks, and even the possibility of having a mixed phase also cannot be ruled out.

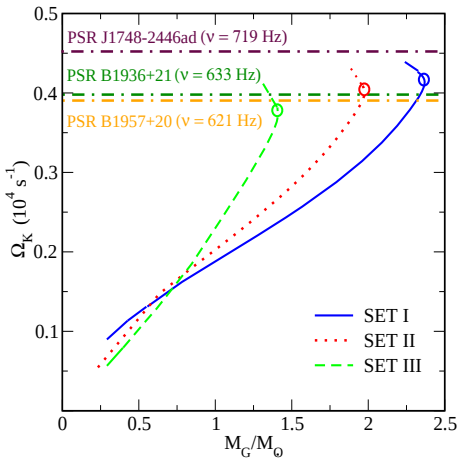

FIG. 4: Keplerian velocity Ω_K $(10^4 S^{-1})$ as a function of the Gravitational mass of the star for EOS with different nucleon effective mass ($^\star/m = 0.80, 0.85$&0.90 as set I, II and III respectively). The Kepler angular velocity obtained for the three cases are 4141 s^{-1}, 3999 s^{-1} and 3714 s^{-1}, which corresponds to a frequency of 659Hz, 636Hz and $591 Hz$. The dot-dashed horizontal lines denotes the observed frequency from the pulsars.

The EOS is the input employed to construct models of rapidly rotating neutron stars. For example, with different EOS of the effective sigma model, we calculated the neutron star properties for both the static and rotating case. In Fig. 4, the keplerian velocity of the star is shown as a function of gravitational mass is plotted for EOS with different nucleon effective mass ($^\star/m = 0.80, 0.85$&0.90 as set I, II and III respectively). Here, we notice an increase of nearly 17-20 % in the star mass, however the central density remains the same. From the observational point of view, we find that recent observations of neutron star masses like $M_{J0751\pm1807}$ $=2.1\pm0.2$ $M_\odot$[30], $M_{4U1636\pm536}=2.0\pm0.1$ $M_\odot$[31], $M_{VelaX-1}=1.86\pm0.16$ $M_\odot$[32] and $M_{VelaX-2}=1.78\pm0.23$ $M_\odot$[33] predicts massive stars. The results of the sigma model are in good agreement with these observations.

TABLE III: Comparison of the static (1st row) and the corresponding rotational (2nd row) attributes of the neutron star predicted with the three parameter sets of the present model.

EOS	$m^\star/m$	M	R_{eq}	$\varepsilon_c/\varepsilon_0$	M_b	P_K
		$(M_\odot)$	(Km)		$(M_\odot)$	(ms)
I	0.80	1.96	17.5	2.85	2.18	–
		2.36	26.4	2.60	2.56	1.52
II	0.85	1.65	16.7	2.96	1.81	–
		1.98	25.5	2.60	2.11	1.57
III	0.90	1.21	15.0	3.45	1.31	–
		1.41	23.7	2.96	1.47	1.69

The crustal effect of the star has also been taken into account by incorporating the BPS EOS [34] at subnuclear densities. As a result of the rotation, the flattening parameter, which is defined as the ratio of the polar to the equatorial radius (R_p/R_e), is ≈ 0.59, at Ω_K. For details of the calculation, one can refer to [13]. The overall global properties for the static and the rotational case for the three EOS is tabulated in Table III.

4. Finite Nuclei

For the sake of completeness, we present few of the finite nuclei results in the Relativistic Mean field framework.

In Fig. 5, the predictions of NL3 for the

Nucleus	BE (MeV)	r_{ch} (fm)	r_n (fm)
^{16}O	−128.83 (−127.62)	2.730 (2.730)	2.580
^{40}Ca	−342.02 (−342.06)	3.469 (3.450)	3.328 (3.370)
^{48}Ca	−415.15 (−416.00)	3.47 0 (3.451)	3.603 (3.625)
^{58}Ni	−503.15 (−506.50)	3.740 (3.769)	3.740 (3.700)
^{90}Zr	−782.63 (−783.90)	4.287 (4.258)	4.306 (4.289)
^{116}Sn	−987.67 (−988.69)	4.611 (4.627)	4.735 (4.692)
^{124}Sn	−1050.18 (−1049.97)	4.661 (4.677)	4.900 (4.851)
^{132}Sn	−1105.44 (−1102.90)	4.709	4.985
^{208}Pb	−1639.54 (−1636.47)	5.520 (5.503)	5.741 (5.593)
^{214}Pb	−1661.62 (−1663.30)	5.581 (5.558)	5.855

FIG. 5: The total binding energies, charge radii, and neutron radii used in the fit (values in parentheses) together with the NL3 predictions [23].

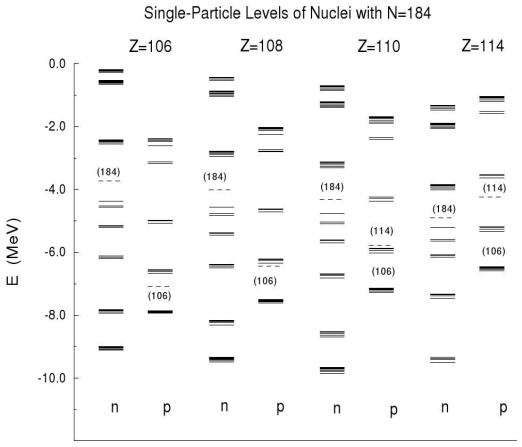

FIG. 6: The neutron and proton single-particle energies for nuclei with Z = 106, 108, 110 and 114 with neutron number N = 184. [35].

ground state properties of some of the nuclei is tabulated. Here we find that the predictions are in very good agreement with the empirical values.

One can also study the single particle energy levels in finite nuclei as well as for nuclei which lies in the superheavy domain of the nuclear chart. As for example, the single-particle levels obtained in the deformed RMF calculations is shown in Figs. 6 both for neutrons and protons corresponding to neutron numbers N=182 for Z=106, 108, 110 and 114. The numbers in the braces shown in the large shell gaps denote shell closures. The associated Fermi energies are also shown by dashed lines. The structure of the single-particle spectra reveals major shell gaps in neutrons at N=166 and at N=184. One of the motivation for studying superheavy nuclei is to analyze new magic numbers.

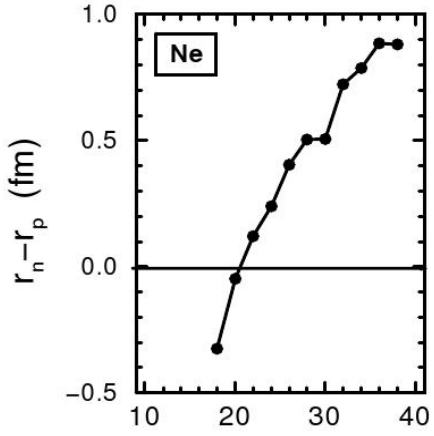

FIG. 7: The neutron skin thickness (proton skin thickness, respectively) $(r_n - r_p)$ as a function of mass A is plotted for neutron rich Ne. [23].

A good description of the various application of the relativistic mean field theory in the finite nuclear domain can be found in [23].

5. Conclusion

For Nuclear matter studies, we employed an effective sigma model and applied the mean-field framework to obtain the EOS of matter with baryons and mesons as the degrees of freedom. One can associate one-to-one correspondence of the model with that of the Relativistic mean-field theory (Walecka model). The model is discussed in relation with the various application of nuclear matter both at low and high densities, and also at finite temperature. In the finite temperature domain we investigated the L-G Phase transition and

found the results to be in agreement with various other theories and experimental observations. With less number of free parameters, we could satisfy the nuclear saturation properties and applied to study the composition and structure of dense matter. As far as the neutron star structure is concerned, the model could account for massive stars, rotating with kepler velocity of $\approx 650Hz$. The results were obtained with EOS which includes the Hyperons and very well compares with recent observations.

For sake of completeness, we highlighted very few results in the finite nuclear domain. RMF has been successful in explaining the isotope shifts of Pb nuclei, which remained intractable for a long time. RMF has also been successfully applied to study the ground-state properties of nuclei near the stability line as well as those close to the neutron and proton drip lines. It has also been applied to investigate the structure of deformed nuclei as well. The ground-state binding energies and charge radii obtained in the RMF theory show a good agreement with the experimental findings. Various interesting phenomenon such as shape co-existence, halo-nuclei, superheavy nuclei etc. has also been studied in RMF. The theory also explains the spherical shape of the nuclei at shell closures or at magic numbers such as 8, 20 and 50. Relativistic mean field RMF theory has gained considerable success in describing various facets of nuclear structure properties. With a limited number of parameters, RMF theory not only satisfies nuclear matter saturation properties but also provides a quantitative description in the finite nuclear domain.

Thus we conclude that the mean-field formalism not only mathematically simplifies the problem, but has been an effective tool to understand and test our knowledge in the nuclear domain.

References

[1] S. Weinberg, Physics **96A**, 327 (1979).

[2] J. D. Walecka, Ann. Phys. **83**, 491 (1974); Phys. Lett. **79B** 10 (1978).

[3] B. D. Serot and J. D. Walecka, Adv. Nucl. Phys. **16**, 1 (1986); Int. J. Mod. Phys. E **6**, 515 (1997).

[4] F. Coester, S. Cohen, B. D. Day and C. M. Vincent, Phys. Rev. C **1** 769 (1970).

[5] R. Machleidt, Adv. Nucl. Phys. **19** 189 (1989).

[6] N. K. Glendening, *Compact stars: Nuclear physics, particle physics, and general relativity*, Springer-Verlag, New York (2000).

[7] S. L Shapiro and S. A. Teukolski, *Black holes, white dwarfs, and Neutron stars*, Wiley, New York, (1983).

[8] N. K. Glendening, Phys. Rev. C **37** 2733 (1988).

[9] W. M. Yao et. al. (Particle Data Group), J. Phys. G **33** 1 (2006) and 2007 partial update for the 2008 edition.

[10] M. Gell-Mann and M. Levy, Nuovo Cim. **16** 705 (1960); T. D. Lee and G. C. Wick, Phys. Rev. D **9** 2291 (1974); J. Boguta, Phys. Lett. B **120** 34 (1983); J. Boguta, Phys. Lett. B **128** 19 (1983).

[11] Volker Koch, *Aspects of Chiral Symmetry*, LBNL-39463/ UC-413.

[12] B. W. Lee, *Chiral Dynamics*, Gordon and Breach, New York (1972).

[13] T. K. Jha, P. K. Raina, P. K. Panda and S. K. Patra, Phys. Rev. **C 74** 055803 (2006); Erratum- Phys. Rev. **C 75** 029903 (2007).

[14] N. K. Glendening, Nucl. Phys. A **480** 597 (1988) .

[15] B. M. Waldhauser, J. A. Maruhn, H. Stöcker and W. Greiner, Phys. Rev. C **38** 1003 (1988); K. C. Chung, C. S. Wang, A. J. Santiago and J. W. Zhang, Eur. Phys. J. A **12** 161 (2001).

[16] P. Möller, W.D. Myers, W.J. Swiatecki and J. Treiner, At. Data Nucl. Data Tables **39** 225 (1988).

[17] C. J. Pethick, D. G. Ravenhall and C. P. Lorenz, Nucl. Phys. A **584**, 675 (1995).

[18] P. Wang, Phys. Rev. C **61**, 054904 (2000).

[19] T. Li *et al.*, Phys. Rev. C **49**, 1630 (1994) .

[20] J. M. Lattimer, and M. Prakash, Phys. Rept., **333**, 121 (2000); J. M. Lattimer, and M. Prakash, Science, **304**, 536 (2004).

[21] P. G. Krastev, and F. Sammarruca, Phys. Rev., C **74** 025808 (2006); H. Heiselberg,

and V. Pandharipande, Ann. Rev. Nucl. Part. Sci., **50**, 481 (2000).
[22] N. Stergioulas and J. L. Friedman, Astrophys. J. **444**, 306 (1995).
[23] G. A. Lalazissis, J. Konig, and P. Ring, Phys. Rev. C **55**, 540 (1997).
[24] G. Q. Li, R. Machleidt and R. Brockmann, Phys. Rev. C **45** 2782 (1992).
[25] C. H. Johnson, D. J. Horen and C. Mahaux, Phys. Rev. C **36**, 2252 (1987).
[26] G. Hua, L. Bo and M. Di Toro, Phys. Rev. C **62**, 035203 (2000).
[27] R. J. Furnstahl and B. D. Serot, Phys. Rev. C **55**, 1499 (1997).
[28] P. K. Sahu, T. K. Jha, K. C. Panda and S. K. Patra, Nucl Phys. A, **733**, 169 (2004).
[29] B. K. Sharma, P. K. Panda, and S. K. Patra, Phys. Rev. C **75**, 035808 (2007).
[30] D. J. Nice, et al. Astrophys. J. **634**, 1242 (2005).
[31] D. Barret, J.F. Olive and M.C. Miller, *astro-ph/0605486*.
[32] O. Barziv, et. al., Astron. Astrophys. **377**, 925 (2001).
[33] J. Casares, P.A. Charles and E. Kuulkers, Astro. J. **493** L39 (1998).
[34] G. Baym, C. Pethick and P. Sutherland, Astrophys. J. **170**, 299 (1971).
[35] G.A. Lalazissis, M. M. Sharma, P. Ring, and Y.K. Gambhir, Nucl. Phys. **A 608**, 202, (1996).